

# Using permutations to quantify and correct for confounding in machine learning predictions

Elias Chaibub Neto<sup>1</sup>

*e-mail:* \* [elias.chaibub.neto@sagebase.org](mailto:elias.chaibub.neto@sagebase.org), <sup>1</sup> Sage Bionetworks

**Abstract:** Clinical machine learning applications are often plagued with confounders that are clinically irrelevant, but can still artificially boost the predictive performance of the algorithms. Confounding is especially problematic in mobile health studies run “in the wild”, where it is challenging to balance the demographic characteristics of participants that self select to enter the study. Here, we develop novel permutation approaches to quantify and adjust for the influence of observed confounders in machine learning predictions. Using restricted permutations we develop statistical tests to detect response learning in the presence of confounding, as well as, confounding learning per se. In particular, we prove that restricted permutations provide an alternative method to compute partial correlations. This result motivates a novel approach to adjust for confounders, where we are able to “subtract” the contribution of the confounders from the observed predictive performance of a machine learning algorithm using a mapping between restricted and standard permutation null distributions. We evaluate the statistical properties of our approach in simulation studies, and illustrate its application to synthetic data sets.

## 1. Introduction

Machine learning algorithms have been increasingly used as diagnostic and prognostic tools in biomedical research. In the emerging field of mobile health, machine learning is especially well positioned to impact clinical research, as the widespread availability of smartphones and other health tracking devices generates high volumes of sensor data that can be readily harnessed to train learners. However, clinical machine learning applications are often plagued with confounding variables that are not clinically relevant, but can still artificially boost the predictive ability of the algorithms.

By definition, a confounder is a variable that is associated with the features (inputs) and the response (outputs) of a classification or regression task. In clinical applications, gender, age, and other demographic characteristics of the study participants often play the role of confounders. Confounding is particularly common in mobile health studies run “in the wild” (i.e., under uncontrolled conditions outside clinical and laboratory settings) where we have little control over the demographic characteristics of the cohort of participants that self-select to participate in the study.

An effective approach to remove the influence of confounders (in predictive settings) is to match samples and balance the data in order to remove the association between confounders and the disease status<sup>1</sup>. The caveat is that we end-up with a smaller number of participants to train and evaluate the machine learning algorithm, and, in highly unbalanced situations, we might end up having to exclude most of the participants from the analyses.

---

<sup>1</sup>Note that including the confounder as an additional feature in the learner does not remove its contribution to the predictive performance. On the contrary, inclusion of a confounder that is highly associated with the response will generally improve the predictive accuracy of the learner, as the confounder alone can be used to predict the response.

To address this drawback, we develop statistical tools to quantify and correct for confounding in machine learning tasks. In particular, we adopt restricted permutations[1] to test if an algorithm is actually learning the response signal (i.e., is able to recognize the labels in a classification problem, or predict a continuous response in regression problems) in addition to learning the signal from the clinically irrelevant confounders. The key idea is to shuffle the response data within the levels of a categorical/ordinal confounder<sup>2</sup> in order to destroy the direct association between the response and the features while still preserving the indirect association mediated by the confounder. Building upon this test, we also develop novel tests to detect confounding per se.

Most importantly, we prove that restricted permutations provide an alternative approach to compute partial correlations (covariances), and develop a novel approach to correct for the influence of the confounders in the predictive performance of machine learning tasks. In addition to the permutation null distribution generated with restricted shufflings of the response data (denoted the “restricted permutation null”), our approach requires the generation of a second null distribution (the “standard permutation null”), where the unrestricted shuffling of the response also destroys the association between response and confounder. The confounding corrected performance score is then obtained by a transformation between these 2 null distributions.

We show via simulations that the empirical type I error rate of the proposed tests are well controlled at the nominal significance levels, and that our correction behaves as expected. We also illustrate the use of the methodology in synthetic data sets.

## 2. The permutation approach

First, we introduce some notation. Throughout the text we let  $m$  represent a predictive performance metric;  $\mathbf{X}$  the feature data matrix;  $\mathbf{y}$  the response data vector; and  $\mathbf{c}$  the observed confounder data vector<sup>3</sup>. We reserve  $F$  to represent a cumulative distribution function (c.d.f.) of an arbitrary random variable, and  $\Phi$  to represent the c.d.f. of a standard normal variable. We let  $F_{\pi^*}$  and  $F_{\pi^{**}}$  represent, respectively, the restricted and standard permutation null distributions (which we describe in the next subsections), and  $\hat{F}_{\pi^*}$  and  $\hat{F}_{\pi^{**}}$  represent the respective Monte Carlo versions of these permutation distributions. We let  $Y^*$  and  $Y^{**}$  represent restricted and standard permutations of the response variable  $Y$ , and  $m^*$  and  $m^{**}$  represent the performance metrics computed with the respective permuted responses. In all analyses presented in this paper, we employ random forest classifiers.

### 2.1. Detecting response learning in the presence of confounding

In statistics, restricted permutations have been used to account for the influence of confounders in randomization tests[1]. Here, we describe how to employ restricted permutations in the context of predictive modeling.

<sup>2</sup>While, in theory we can only perform the restricted permutations using categorical/ordinal confounders, in practice we can always discretize and evaluate continuous confounders as well.

<sup>3</sup>Note that if multiple confounders are available, than  $\mathbf{c}$  can represent the combined categorical confounder vector, generated by pasting together the multiple confounder vectors. For instance, if our confounders are a discretized age variable with levels “young”, “middle age”, and “senior”, and a gender variable with levels “male” and “female”, then the combined confounder has the following six levels: “young male”, “young female”, “middle age male”, “middle age female”, “senior male”, and “senior female”.

When the relationship between the features,  $\mathbf{X}$ , and the response,  $\mathbf{y}$ , is influenced by an observed set of confounders,  $\mathbf{c}$ , the total association between  $\mathbf{X}$  and  $\mathbf{y}$  can be partitioned into a component due to the direct association between  $\mathbf{X}$  and  $\mathbf{y}$  (due to a potential causal relation between  $\mathbf{y}$  and  $\mathbf{X}$ , or to the presence of additional unmeasured confounders associated with  $\mathbf{X}$  and  $\mathbf{y}$ ), and into an indirect component where part of the association between features and response is explained by the association between  $\mathbf{X}$  and  $\mathbf{c}$ , and the association between  $\mathbf{c}$  and  $\mathbf{y}$ . Figure 1a provides a graphical model representation of these associations.

In order to evaluate whether a machine learning algorithm has learned about the response variable (even when confounding is present) we need to generate a permutation null distribution where the direct association between the response and the features is destroyed, while the indirect association mediated by the confounder is still preserved (Figure 1b). To this end, we generate a restricted permutation null distribution (as described in Algorithm 1) by separately shuffling the response data within each level of the confounder (as illustrated in Figure 1e-g).

---

**Algorithm 1** Restricted Monte Carlo permutation null distribution for metric  $m$

---

```

1: Input: Number of permutations,  $b$ ;  $\mathbf{X}$ ;  $\mathbf{y}$ ;  $\mathbf{c}$ ; training and test set indexes,  $i_{train}, i_{test}$ 
2: Split  $\mathbf{X}$ ,  $\mathbf{y}$  and  $\mathbf{c}$  into training and test sets
3: for  $i = 1, 2, \dots, b$  do
4:    $\mathbf{y}_{train}^* \leftarrow \text{RestrictedShuffle}(\mathbf{y}_{train}, \mathbf{c}_{train})$ , and  $\mathbf{y}_{test}^* \leftarrow \text{RestrictedShuffle}(\mathbf{y}_{test}, \mathbf{c}_{test})$ 
5:   Train a machine learning algorithm on the  $\mathbf{X}_{train}$  and  $\mathbf{y}_{train}^*$  data
6:   Evaluate the algorithm on the  $\mathbf{X}_{test}$  and  $\mathbf{y}_{test}^*$  data
7:   Record the value of the performance metric,  $m_i^*$ , on the shuffled data
8: end for
9: Output:  $m_1^*, m_2^*, \dots, m_b^*$ 

```

---

Supplementary Figure S1 show examples of the restricted permutation null distributions (for the AUC metric) generated with varying amounts of confounding. These examples show that the restricted permutation null is always centered away from the baseline random guess value whenever confounding is present, and illustrate that this shift can be used to informally infer the presence of confounding.

The restricted Monte Carlo permutation null allows us to test the hypotheses,

- $H_0^*$  : the machine learning algorithm is not learning the response signal,
- $H_1^*$  : the machine learning algorithm is learning the response signal.

A permutation p-value for testing  $H_0^*$  is computed as the proportion of times that the performance metric computed in shuffled response data was equal or better than the performance metric computed with the original (un-shuffled) response vector,  $m_o$ . (Figure S1 provide some examples.)

## 2.2. Correcting for the influence of confounders in machine learning predictions

Let  $E_{\pi^*}[M^*]$  represent the expectation of the restricted permutation null distribution. This quantity represents a natural candidate to measure the contribution of confounding to the learner’s predictive ability, as it measures the algorithm’s performance after the algorithm’s ability to learn the direct association between the response and the features has been neutralized by the restricted shuffling of the response data. The observed metric value,  $m_o$ ,

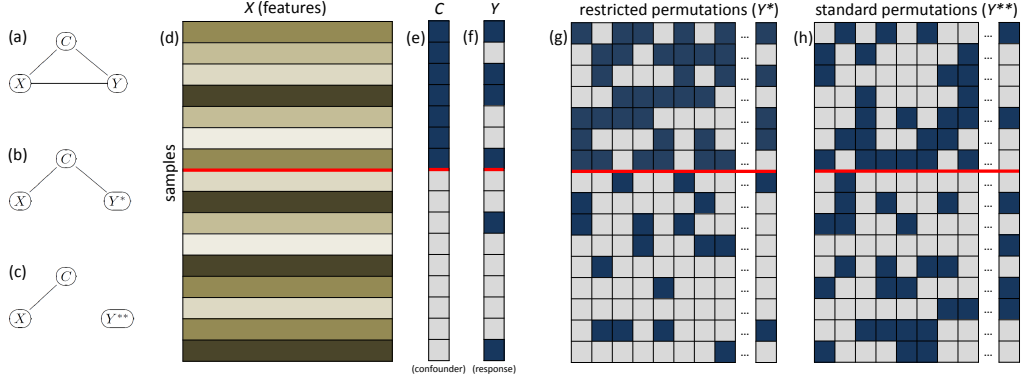


FIG 1. Panel a shows an undirected dependency graph (UDG) representing the associations between the features,  $X$ , the response,  $Y$ , and the observed confounders,  $C$ . (In an UDG, an undirected edge between two nodes means that the variables are associated even when we condition on the remaining variables.) Panels d, e, and f, represent the feature, confounder, and response data, respectively. In this cartoon example, we have 16 samples, and both  $C$  and  $Y$  are binary (light and dark cells represent 0 and 1 values, respectively). The confounder vector (panel e) was sorted, and the red line splits the data relative to the levels of  $C$  (i.e., the top 7 samples have confounding value 1, while the bottom 9 have confounding value 0). Note that in panel f we have 4 positive response values (dark cells) above the red line, and 2 below it. Panel g illustrates the restricted permutation scheme. Each column shows a distinct permutation. In all permutations, we still have 4 dark cells above the red line and 2 below it. Panel b shows the UDG representation of these relations (note that conditional on the confounder the features and the restricted shuffled response,  $Y^*$ , become independent). Panel h illustrates the standard permutation scheme, where we shuffle the response values freely across the entire response vector (now, each column is no longer constrained to have 4 dark cells above the red line and 2 below it). The standard permutations destroy the association between  $Y$  and  $C$  and between  $Y$  and  $X$ . Panel c shows the UDG representation in this case.

on the other hand, captures the contributions of both response learning and confounder learning to the predictive performance. It is reasonable to expect that the contribution of the response alone should be a function of the difference between  $m_o$  and  $E_{\pi^*}[M^*]$ , and we would intuitively expect that the corrected performance metric,  $m_c$ , to assume the form,

$$m_c = f(m_o - E_{\pi^*}[M^*]) . \quad (1)$$

As a matter of fact, the following result (proved in the Supplement) formalizes this intuition for linear measures of statistical association.

**Theorem 1.** Let  $C$  represent a categorical variable,  $X$  and  $Y$  represent arbitrary random variables, and  $Y^*$  represent a restricted permutation of  $Y$  relative to the levels of  $C$ . Let  $\text{Cov}(X, Y)$  represent the covariance between  $X$  and  $Y$ , and  $\text{Cov}(X, Y | C)$  represent the partial covariance between  $X$  and  $Y$  given  $C$ . An alternative formula for the computation of  $\text{Cov}(X, Y | C)$ , based on the restricted permutations of  $Y$  with respect to the levels of  $C$ , is given by,

$$\text{Cov}(X, Y | C) = \text{Cov}(X, Y) - E_{\pi^*}[\text{Cov}(X, Y^*)] .$$

Similarly, the partial correlation  $\text{Cor}(X, Y | C)$  can be expressed as,

$$\text{Cor}(X, Y | C) = \left( \frac{\text{Var}(X) \text{Var}(Y)}{\text{Var}(X | C) \text{Var}(Y | C)} \right)^{\frac{1}{2}} (\text{Cor}(X, Y) - E_{\pi^*}[\text{Cor}(X, Y^*)]) .$$

Note that, for the covariance metric the function  $f()$  in equation (1) corresponds to the identity function, while for the correlation metric it simply re-scales the difference  $m_o - E_{\pi^*}[M^*]$ .

Theorem 1 shows that the total amount of linear association between two arbitrary random variables measured by  $Cov(X, Y)$  can be partitioned into the  $E_{\pi^*}[Cov(X, Y^*)]$  component, that measures the amount of association between  $X$  and  $Y$  that is due exclusively to the confounder  $C$  (i.e., the indirect association), and into the  $Cov(X, Y | C)$  component, that measures the remaining amount of association between  $X$  and  $Y$  that is not explained by the confounder  $C$  (i.e., the direct association).

We point out, however, that the above result is not exclusively available for linear measures of association. In the Supplement, we also present and prove a similar result (Theorem 2) involving the distance correlation[2] and partial distance correlation[3], showing that the restricted permutations can also be used to decompose non-linear measures of statistical association.

Motivated by these results, we now propose a general approach to compute the corrected performance metric,  $m_c$ , for an arbitrary metric  $m$ . It requires, however, the computation of a second permutation distribution,  $F_{\pi^{**}}$ , denoted the “standard” permutation null, that is generated in the usual way by freely shuffling the response values across the entire response vector (Figure 1h). Note that the standard shuffling destroys the association between the response and the features, as well as, the association between the response and the confounder (Figure 1c), and can be used to test the hypotheses,

- $H_0^{**}$  : the algorithm is not learning the response and confounding signals
- $H_1^{**}$  : the algorithm is learning the response and/or the confounding signal.

A Monte Carlo estimate of the standard permutation null is generated as described in Algorithm 1, except that the restricted shuffling of the response data in step 4 is replaced by standard shuffling.

### 2.2.1. The confounding corrected metric

As pointed before, the observed metric  $m_o$  captures the contributions of both response and confounder learning. In order to estimate the confounding corrected value  $m_c$  we need to determine what value would the observed performance metric have assumed, had the response variable not been associated with the confounder. In other words we need to map a value sampled from a distribution where the response and confounder are associated to a distribution where they are not.

To this end, we construct a mapping from the restricted permutation null distribution (where the association between the response and the confounder is preserved) to the standard permutation null (where this association is removed). Hence, we estimate  $m_c$  by equating  $F_{\pi^{**}}(m_c)$  to  $F_{\pi^*}(m_o)$ ,

$$F_{\pi^{**}}(\hat{m}_c) = F_{\pi^*}(m_o) \Leftrightarrow \hat{m}_c = F_{\pi^{**}}^{-1}(F_{\pi^*}(m_o)) . \quad (2)$$

Note that equating  $F_{\pi^*}(m_o)$  to  $F_{\pi^{**}}(m_c)$  is equivalent to equating the p-value for testing  $H_0^*$  vs  $H_1^*$  to the p-value for testing  $H_0^{**}$  vs  $H_1^{**}$ <sup>4</sup>.

<sup>4</sup>For metrics where smaller values indicate better predictive performance (e.g., mean squared error) we have that  $F_{\pi^*}(m_o)$  corresponds to the p-value for testing  $H_0^*$ . For metrics where larger values indicate better performance (e.g, AUC), the p-value is given by  $1 - F_{\pi^*}(m_o)$ , and we get the same correction formula by matching this p-value to  $1 - F_{\pi^{**}}(m_c)$ .

In general, it is unfeasible to simulate  $F_{\pi^*}$  and  $F_{\pi^{**}}$  exactly due the large number of possible permutations. Presumably, one could rely on Monte Carlo estimates of these distributions and estimate  $m_c$  as  $\hat{m}_c = \hat{F}_{\pi^{**}}^{-1}(\hat{F}_{\pi^*}(m_o))$ , where  $\hat{F}_{\pi^*}(x)$  represents the  $x$ th sample percentile of the Monte Carlo restricted null, and  $\hat{F}_{\pi^{**}}^{-1}(x)$  represents the  $x$ th sample quantile of the Monte Carlo standard null. Observe, however, that this approach only works when  $m_o$  falls inside the range of  $\hat{F}_{\pi^*}$ . As illustrated in Figure S2, the corrected metric value gets artificially “truncated” whenever the observed correlation is outside the range of the restricted permutation null. Therefore, in practice, we need to use analytical approximations for the restricted and standard permutation null distributions in order to estimate  $m_c$ .

Fortunately, because popular performance metrics such as the mean square error, mean absolute error, and the classification accuracy correspond to averages, while metrics such as the AUC correspond to a generalized U-statistics[4, 5], we have that the distribution of these statistics can be well approximated by Gaussian distributions when the test set is large enough (due to central limit theorems associated with averages, and to the asymptotic normality of (generalized) U-statistics[6, 7]). Figures S3 and S4 provide a few illustrative examples. Hence, in practice, we will often be able to approximate  $\hat{F}_{\pi^*}$  and  $\hat{F}_{\pi^{**}}$  by,

$$\hat{F}_{\pi^*} \approx N(a_{\hat{\pi}^*}, s_{\hat{\pi}^*}^2), \quad \hat{F}_{\pi^{**}} \approx N(a_{\hat{\pi}^{**}}, s_{\hat{\pi}^{**}}^2), \quad (3)$$

where  $a_{\hat{\pi}^*}$  and  $a_{\hat{\pi}^{**}}$  correspond, respectively, to the sample mean of  $\hat{F}_{\pi^*}$  and  $\hat{F}_{\pi^{**}}$ , and  $s_{\hat{\pi}^*}^2$  and  $s_{\hat{\pi}^{**}}^2$  represent the respective sample variances. Now, by replacing  $F_{\pi^*}$  and  $F_{\pi^{**}}$  in equation (2) by the approximate Gaussian distributions in (3) we have that,

$$\hat{F}_{\pi^{**}}(\hat{m}_c) \approx \Phi\left(\frac{\hat{m}_c - a_{\hat{\pi}^{**}}}{s_{\hat{\pi}^{**}}}\right) = \Phi\left(\frac{m_o - a_{\hat{\pi}^*}}{s_{\hat{\pi}^*}}\right) \approx \hat{F}_{\pi^*}(m_o), \quad (4)$$

and we can estimate  $\hat{m}_c$  by,

$$\hat{m}_c = (m_o - a_{\hat{\pi}^*}) \frac{s_{\hat{\pi}^{**}}}{s_{\hat{\pi}^*}} + a_{\hat{\pi}^{**}}. \quad (5)$$

Note that the above correction formula still have the same format as equation (1), with  $f()$  performing a re-scaling and translation of the difference  $m_o - \hat{E}_{\hat{\pi}^*}[M^*]$ . Furthermore, for the correlation metric,  $a_{\hat{\pi}^{**}} = \hat{E}_{\hat{\pi}^{**}}[M^{**}] \approx 0$ , and the correction has similar format as the formula in Theorem 1.

Figure 2a illustrates the application of formula 5 to the correlation metric. Figure 2b illustrates that the correction formula (x-axis) was able to recapitulate very well the sample partial correlation values (y-axis), computed as,

$$\hat{c}or(X, Y | C) = \frac{\hat{c}or(X, Y) - \hat{c}or(X, C) \hat{c}or(Y, C)}{\sqrt{(1 - \hat{c}or(X, C)^2)(1 - \hat{c}or(Y, C)^2)}}. \quad (6)$$

For completeness, Figure 2c compares the partial correlation values computed with the sample version of the formula presented in Theorem 1, against the sample partial correlation values.

### 2.3. A statistical test to detect confounding

As described before, the presence of confounding will shift the restricted permutation null distribution away from the baseline random guess value, and this shift can be used to

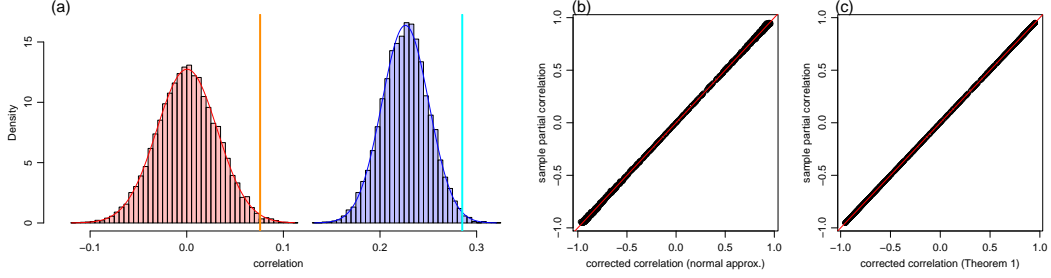


FIG 2. Panel a shows an example of the restricted (blue) and standard (red) Monte Carlo permutation null distributions for the correlation metric (see the Supplement for the simulation details). The cyan line shows the observed correlation, while the orange one shows the corrected correlation value (from formula 5). The blue and red curves correspond to the normal approximations in eq. (3). Note that the tail probabilities to the right of the cyan and orange lines are the same (i.e., the p-values are preserved). Panels b and c compare our correction formulas against the sample partial correlation.

informally infer the presence of confounding. Here, we present a hypothesis test to formally test the hypotheses,

$H_0^c$  : the machine learning algorithm has not learned the confounding signal

$H_1^c$  : the machine learning algorithm has learned the confounding signal.

We adopt the sample mean of the restricted permutation null,

$$\bar{M}^* = \frac{1}{b} \sum_{i=1}^b M_i^*, \quad (7)$$

as a test statistic, since it represents a natural measure of confounding. Note that under the null hypothesis that an algorithm has not learned the confounding signal, the restricted permutation null will have the same distribution as the standard permutation null. Hence, for large enough test sets we have that  $M^* \approx N(a_{\hat{\pi}^{**}}, s_{\hat{\pi}^{**}}^2)$ , and our test statistic is asymptotically distributed as,

$$\bar{M}^* \approx N\left(a_{\hat{\pi}^{**}}, \frac{s_{\hat{\pi}^{**}}^2}{b}\right). \quad (8)$$

Note that the variance of this null distribution depends on the number of permutations ( $b$ ) used to generate the restricted permutation null, and gets smaller as we increase  $b$ . As a consequence, we can easily obtain a statistically significant result by increasing the number of permutations<sup>5</sup>. In order to avoid this artifact, we restrict  $b$  to be equal to the size of the test set. By doing so, we guarantee that we will only be able to detect small confounding effects when we are truly well powered to do so. In Section 3, we report the results of a simulation study evaluating the empirical performance of the confounding test (Figure 3b), where we set the number of permutations to be equal to the test set sample size. We observed

<sup>5</sup>For instance, suppose we are working on a classification problem using the AUC metric, and the sample average of the restricted permutation null,  $\bar{auc}^*$ , is given by 0.51. If the confounding effect is small but real, we can improve the test's statistical significance by increasing the number of permutations, since our test statistic estimate will converge to a small but larger than 0.5 value, while the confounding null distribution will get more and more peaked around 0.5 (the baseline random guess value for the AUC metric).

good power to detect confounding under  $H_1^c$ , and well controlled type I error rates under  $H_0^c$ .

In the Supplement, we also present a general permutation scheme (Algorithm 2) that does not require asymptotic normality assumption, and can be used with small test sets.

#### 2.4. Analytical results for the AUC metric

It has been shown[8] that, when there are no ties in the predicted class probabilities used for the computation of the *AUC*, the test statistic of the Wilcoxon rank sum test (also known as the Mann-Whitney U test),  $U$ , is related to the *AUC* statistic by,  $U = n_n n_p (1 - AUC)$ , where  $n_n$  and  $n_p$  represent the number of negative and positive labels in the test set (see Section 2 of reference[9] for details).

For large test sets, and under the null hypothesis  $H_0^{**}$  (i.e., that the machine learning algorithm has not learned the response and the confounding signal), this distribution can be approximated[9] by

$$U \approx N \left( \frac{n_n n_p}{2}, \frac{n_n n_p (n_n + n_p + 1)}{12} \right). \quad (9)$$

Now, from the relation  $AUC = 1 - U/(n_n n_p)$  it follows that,

$$AUC \approx N \left( \frac{1}{2}, \frac{n_n + n_p + 1}{12 n_n n_p} \right), \quad (10)$$

under the null  $H_0^{**}$ , so that  $F_{\pi^{**}}$  can be approximated by the above normal distribution.

Using the ‘‘p-value matching’’ criterion,  $F_{\pi^{**}}(auc_c) = F_{\pi^*}(auc_o)$ , it follows that,

$$\Phi \left( \frac{auc_c - 0.5}{\sigma} \right) \approx F_{\pi^*}(auc_o) \Leftrightarrow auc_c \approx \Phi^{-1}(F_{\pi^*}(auc_o)) \sigma + 0.5, \quad (11)$$

where  $\Phi$  represents the cumulative density function of a standard normal random variable, and  $\sigma = \sqrt{(n_n + n_p + 1)/(12 n_n n_p)}$ .

Now, observe that because the *AUC* is a generalized U-statistic [5, 7] it will also be asymptotically distributed as a normal random variable (even under the alternative). Hence, for large sample sizes,

$$F_{\pi^*} \approx N(a_{\hat{\pi}^*}, s_{\hat{\pi}^*}^2), \quad a_{\hat{\pi}^*} = \hat{E}_{\hat{\pi}^*}[AUC^*], \quad s_{\hat{\pi}^*}^2 = \hat{Var}_{\hat{\pi}^*}(AUC^*), \quad (12)$$

where  $\hat{E}_{\hat{\pi}^*}$  and  $\hat{Var}_{\hat{\pi}^*}$  represent the sample average and sample variance of the restricted permutation null distribution of *AUC* scores. The confounder corrected *AUC* score is then estimated as,

$$auc_c = (auc_o - a_{\hat{\pi}^*}) \frac{n_n + n_p + 1}{12 n_n n_p s_{\hat{\pi}^*}} + 0.5. \quad (13)$$

<sup>6</sup>In the presence of ties, a slightly better approximation, is given by,

$$U \approx N \left( \frac{n_n n_p}{2}, \frac{n_n n_p (n_n + n_p + 1)}{12} - \frac{n_n n_p}{12 n (n - 1)} \sum_{k=1}^{\tau} t_k (t_k - 1)(t_k + 1) \right),$$

where  $\tau$  is the number of groups of ties, and  $t_k$  is the number of ties in group  $k$ [9]. We have compared both approximations and did not detect any discernible differences in the results. For this reason, we adopted the simpler approximation in equation (9).

Furthermore, under the null hypothesis that the classifier has not learned the confounding signal, it follows that the confounding null distribution for the test statistic  $AUC^* = b^{-1} \sum_{i=1}^b AUC_i^*$  is given by,

$$N\left(\frac{1}{2}, \frac{n_n + n_p + 1}{12 n_n n_p b}\right). \quad (14)$$

### 3. Simulation experiments

Figure 3 reports the results from four simulation experiments based on data generated with: disease and confounding signal ( $H_1^*$  and  $H_1^c$ ); disease but no confounding signal ( $H_1^*$  and  $H_0^c$ ); no disease or confounding signal ( $H_0^*$  and  $H_0^c$ ); and confounding but no disease signal ( $H_0^*$  and  $H_1^c$ ). See Supplement for the simulation details. In each experiment we generated 1,000 data sets and recorded the proportion of times that we rejected the null hypothesis across a grid of nominal significance levels varying from 0 to 1. Note that this proportion represents the empirical type I error rate when the data is simulated under the null, but the empirical power when the data is simulated under the alternative.

Panel a reports the power/error rate curves for the  $H_0^*$  vs  $H_1^*$  test. The blue and red curves represent the experiments with data simulated under  $H_1^*$ , and show that the restricted permutation test is well powered to detect disease learning in the presence (blue) or absence (red) of confounding. The green and black curves represent the simulation experiments under  $H_0^*$  and show that the error rates are well controlled at the nominal significance levels in the presence (green) or absence (black) of confounding. (Note that a type I error rate curve close to the diagonal line implies that the distribution of the p-values is close to a uniform distribution in the 0 to 1 interval.)

Panel b reports the same results for the  $H_0^c$  vs  $H_1^c$  test. Again we observe well controlled errors under  $H_0^c$  in the presence (red) and absence (black) of disease signal, and good power to detect confounding under  $H_1^c$ .

Panels c-f show the distributions of the observed (cyan) and corrected (orange) AUCs for each of the 4 simulation experiments. In the presence of confounding (panels c and e), the corrected AUCs were lower than the observed AUCs, while in the absence of confounding (panels d and f), the corrected AUCs closely matched the observed values. Note, as well, that under  $H_0^*$  the corrected AUCs were distributed around 0.5 (panels e and f), while the observed AUCs were still above of 0.5 in panel e due to confounding.

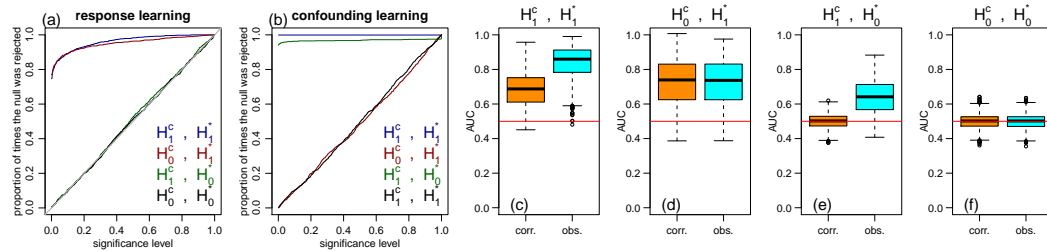


FIG 3. Simulation study. The corrected AUCs and confounding tests were based on the analytical results described in Section 2.4. In each simulation, the number of permutations was set to equal the test set size.

#### 4. Discussion

In statistics, restricted permutations have been widely used in the analysis of complex experimental designs (in order to maintain the validity of the exchangeability assumption and guarantee the exactness of randomization tests[10]). Restricted permutations have also been used to adjust for the influence of confounders in randomization tests[1]. Here, we apply and evaluate the statistical properties of restricted permutations in the context of predictive modeling. Note that the only assumption required to guarantee the exactness of the test is that, under  $H_0^*$ , the response data is exchangeable within each level of the (combined) confounder variable. The test does not require any distributional assumptions and is applicable to any performance metric in both regression and classification problems.

We also propose and evaluate novel hypothesis tests to detect confounding. Together, the restricted permutation tests and confounding tests provide a principled and direct approach to check if potential confounders are truly influencing the predictive performance of a learner. Recall that demographic variables associated with the response, but not with the features, will not confound the prediction. Hence, the proposed tests can be used to assess which potential confounders are really problematic.

If an important confounder is detected, then the novel correction approach propose in this paper can be used to estimate how much the algorithm has actually learned about the response. Observe, however, that this correction is done “after the fact”, when the algorithm has already had a chance to learn both response and confounding signals (and, perhaps, has learned the confounding signals better than the response signal). Ideally, one should try to prevent an algorithm from learning the confounding signal in the first place. While sample matching can be used to this end, it can also drastically reduce the size of the training and test sets. Therefore, we might still obtain a better predictive performance (after correcting for the confounder) by training the learner with the entire data set, rather than with the reduced matched set. Of course, there are situations where the reverse is true. (See Figure S5 for a simulation study comparing our correction vs the matching approach.)

In a previous contribution[11], we proposed permutation tests to detect disease signal in the presence of “identity confounding”<sup>7</sup>, as well as, permutation tests to detect the “identity confounding” itself. That work, however, relies in a different permutation strategy (i.e., “subject-wise” label shufflings), rather than the restricted permutations adopted in this paper.

Finally, we point out that a key application for the methodology proposed in this paper is the assessment of “digital biomarkers”[12, 13, 14] (i.e., features generated from sensor data that can objectively detect the disease signal) in mobile health studies. At its core, the development of digital biomarkers involves the generation and comparison of distinct sets of features, including features engineered manually by signal processing experts, as well as, features learned automatically by deep models. Ideally, a digital biomarker should be able to detect disease signals, but not confounding signals. Hence, it is essential to evaluate whether, and to what degree, these features are truly able to detect disease signals, rather than, say, age and gender signals. We anticipate that the methodology developed in this paper will provide an important tool for researchers in this field.

---

<sup>7</sup>The “identity confounding” issue arises when the relationship between the features and the disease labels learned by a classifier is confounded by the identity of the subjects. This problem can arise in mobile health studies where the longitudinal records provided by each participant are split into the training and test sets (record-wise data split), rather than being assigned to either the training or the test sets (subject-wise data split). When data from each participant is present in both the training and test sets, the classifier might be mostly learning about the subject’s individual characteristics rather than the disease signature.

## References

- [1] Good, P. (2000) *Permutation tests: a practical guide to resampling methods for testing hypothesis*. 2nd ed. Springer, New Yourk.
- [2] Szekely, G., Rizzo, M. L., Bakirov, N. K. (2007) Measuring and testing dependence by correlation of distances. *Annals of Statistics* **35**: 2769-2794.
- [3] Szekely, G. & Rizzo, M. L. (2014) Partial distance correlation with methods for dissimilarities. *Annals of Statistics* **42**: 2382-2412.
- [4] DeLong, E. R., DeLong, D. M. & Clarke-Pearson, D.L. (1988) Comparing the areas under two or more correlated receiver operating characteristic curves: a nonparametric approach. *Biometrics* **44**: 837-845.
- [5] Lehmann, E. L. (1951) Consistency and unbiasedness of certain nonparametric tests. *Annals of Mathematical Statistics* **22**: 165-179.
- [6] Hoeffding, W. (1948) A class of statistics with asymptotically normal distribution. *Annals of Mathematical Statistics* **19**: 293-325.
- [7] Serfling, R. J. (1980) *Approximation theorems of mathematical statistics*. Jowh Wiley & Sons.
- [8] Bamber, D. (1975) The area above the ordinal dominance graph and the area below the receiver operating characteristic graph. *Journal of Mathematical Psychology* **12**: 387-415.
- [9] Mason, S. L. & Graham, N. E. (2002) Areas beneath the relative operating characteristics (ROC) and relative operating levels (ROL) curves: statistical significance and interpretation. *Quarterly Journal of the Royal Meteorological Society* **128**: 2145-2166.
- [10] Anderson, M. J. & Ter Braak C. J. F. (2003) Permutation tests for multi-factorial analysis of variance. *Journal of Statistical Computation and Simulation* **73**: 85-113.
- [11] Chaibub Neto, E., et al. (2017) Detecting confounding due to subject identification in clinical machine learning diagnostic applications: a permutation test approach. [arXiv:1712.03120](https://arxiv.org/abs/1712.03120).
- [12] Dorsey, R. E., Papapetropoulos, S., Xiong, M. & Kieburz K. (2017) The first frontier: digital biomarkers for neurodegenerative disorders. *Digital Biomarkers* **1**: 6-13.
- [13] Rodarte, C. (2017) Pharmaceutical perspective: how digital biomarkers and contextual data will enable therapeutic environments. *Digital Biomarkers* **1**: 73-81.
- [14] Dagum, P. (2018) Digital biomarkers of cognitive function. *npj Digital Medicine* **1**: doi:10.1038/s41746-018-0018-4
- [15] Dai, B., Ding, S., & Wahba, G. (2013) Multivariate Bernoulli distribution. *Bernoulli* **19**:1465-1483.
- [16] Santner, T.J., Williams, B.J. & Notz, W.I. (2003). *The Design and Analysis of Computer Experiments*. Springer Verlag, New York.
- [17] Johnson, M., Moore, L. & Ylvisaker, D. (1990). Minimax and maximin distance designs. *Journal of Statistical Planning and Inference*, **26**, 131-148.

## SUPPLEMENT

### 5. Proof of Theorem 1

Let's start with the covariance operator. By definition,

$$\text{Cov}(X, Y | C) = \text{Cov}(X, Y) - \text{Cov}(X, C) \text{Var}(C)^{-1} \text{Cov}(Y, C) . \quad (15)$$

Hence,

$$Cov(X, Y^* | C) = Cov(X, Y^*) - Cov(X, C) Var(C)^{-1} Cov(Y^*, C) , \quad (16)$$

and

$$E_{\pi^*} [Cov(X, Y^* | C)] = E_{\pi^*} [Cov(X, Y^*)] - E_{\pi^*} [Cov(X, C) Var(C)^{-1} Cov(Y^*, C)] , \quad (17)$$

where the expectation is taken with respect to the restricted permutation null distribution,  $F_{\pi^*}$ .

Now, recall that  $Cov(X, Y)$  measures the total amount of association between  $X$  and  $Y$ , which can be partitioned into a the component due to the direct association between  $X$  and  $Y$  (due to a potential causal relation between these two variables, or to the presence of additional unmeasured confounders associated with  $X$  and  $Y$ ) and into an indirect component where part of the association between  $X$  and  $Y$  is explained by the association between  $X$  and  $C$ , and between  $C$  and  $Y$ . Because the restricted shuffling of  $Y$  with the respect to the levels of  $C$  preserves the associations between  $Y$  and  $C$  and between  $X$  and  $C$ , we have that the restricted shuffling removes the direct association between  $X$  and  $Y$ , leaving intact the indirect association component mediated by  $C$ . In other words, the average association between  $X$  and  $Y^*$  (across all possible restricted permutations of  $Y$ ) is completely explained by  $C$ . Hence, it follows that conditional on  $C$ , this average association vanishes, that is,

$$E_{\pi^*} [Cov(X, Y^* | C)] = 0 , \quad (18)$$

so that,

$$\begin{aligned} E_{\pi^*} [Cov(X, Y^*)] &= E_{\pi^*} [Cov(X, C) Var(C)^{-1} Cov(Y^*, C)] \\ &= E_{\pi^*} [Cov(X, C) Var(C)^{-1} Cov(Y, C)] \\ &= Cov(X, C) Var(C)^{-1} Cov(Y, C) , \end{aligned} \quad (19)$$

where the second equality follows from the fact that  $Cov(Y^*, C) = Cov(Y, C)$ . Therefore, it follows from (15) and (19) that,

$$Cov(X, Y | C) = Cov(X, Y) - E_{\pi^*} [Cov(X, Y^*)] . \quad (20)$$

To prove the result for the partial correlation, observe that by dividing the above equation by  $\sqrt{Var(X)Var(Y)}$ , and recalling that by definition  $Cor(X, Y) = Cov(X, Y)/\sqrt{Var(X)Var(Y)}$  we have that,

$$\begin{aligned} \frac{Cov(X, Y | C)}{\sqrt{Var(X)Var(Y)}} &= Cor(X, Y) - E_{\pi^*} \left[ \frac{Cov(X, Y^*)}{\sqrt{Var(X)Var(Y)}} \right] , \\ &= Cor(X, Y) - E_{\pi^*} [Cor(X, Y^*)] , \end{aligned} \quad (21)$$

where the second equality follows from the fact that  $Var(Y) = Var(Y^*)$ . Now, recalling that by definition  $Cor(X, Y | C) = Cov(X, Y | C)/\sqrt{Var(X | C)Var(Y | C)}$ , the result follows by dividing and multiplying the left hand side of the above equation by  $\sqrt{Var(X | C)Var(Y | C)}$  and rearranging terms.

## 6. Theorem 2

**Theorem 2.** *Let  $C$  represent a categorical variable,  $X$  and  $Y$  represent arbitrary random variables, and  $Y^*$  represent a restricted permutation of  $Y$  relative to the levels of  $C$ . Let  $dCov(X, Y)$  represent the distance covariance between  $X$  and  $Y$ , and  $dCov(X, Y | C)$  represent the partial distance covariance between  $X$  and  $Y$  given  $C$ . An alternative formula for the computation of  $dCov(X, Y | C)$ , based on the restricted permutations of  $Y$  with respect to the levels of  $C$ , is given by,*

$$dCov(X, Y | C) = dCov(X, Y)^2 - E_{\pi^*} [dCov(X, Y^*)^2] . \quad (22)$$

Similarly, the partial distance correlation  $dCor(X, Y | C)$  can be expressed as,

$$dCor(X, Y | C) = \frac{dCor(X, Y)^2 - E_{\pi^*} [dCor(X, Y^*)^2]}{\sqrt{(1 - dCor(X, C)^4)(1 - dCor(Y, C)^4)}} . \quad (23)$$

### 6.1. Proof of Theorem 2

Consider first the partial distance covariance operator. By definition (see equation A.1 in Appendix A.5 of reference[3]),

$$dCov(X, Y | C) = dCov(X, Y)^2 - dCov(X, C)^2 dVar(C)^{-2} dCov(Y, C)^2 . \quad (24)$$

Following the same reasoning used in the proof of Theorem 1 we obtain equation (22).

Now, let's consider the partial distance correlation. By definition the distance correlation is given by[2],

$$dCor(X, Y) = \frac{dCov(X, Y)}{\sqrt{dVar(X) dVar(Y)}} . \quad (25)$$

Dividing equation (22) by  $dVar(X) dVar(Y)$  we have that

$$\frac{dCov(X, Y | C)}{dVar(X) dVar(Y)} = dCor(X, Y)^2 - E_{\pi^*} \left[ \frac{dCov(X, Y^*)^2}{dVar(X) dVar(Y)} \right] , \quad (26)$$

$$= dCor(X, Y)^2 - E_{\pi^*} [dCor(X, Y^*)^2] , \quad (27)$$

where the second equality follows from the fact that  $dVar(Y) = dVar(Y^*)$ .

By definition the partial distance correlation (see Appendix A.5 of reference[3]) is given by,

$$dCor(X, Y | C) = \frac{dCov(X, Y | C)}{\sqrt{dVar(X)^2(1 - dCor(X, C)^4) dVar(Y)^2(1 - dCor(Y, C)^4)}} . \quad (28)$$

Hence, we obtain the result in equation (23) by dividing and multiplying the left hand side of equation (27) by  $\sqrt{dVar(X)^2(1 - dCor(X, C)^4) dVar(Y)^2(1 - dCor(Y, C)^4)}$  and rearranging terms.

### 7. Algorithm 2

In order to test whether a machine learning algorithm is learning the confounding signal, we need to generate a permutation null distribution (for the  $\bar{m}^*$  statistic) where the indirect association mediated by the confounder is destroyed. To this end, we shuffle the confounder vector in a standard fashion, before computing the  $\bar{m}^*$  statistic, as described in Algorithm 2 below.

---

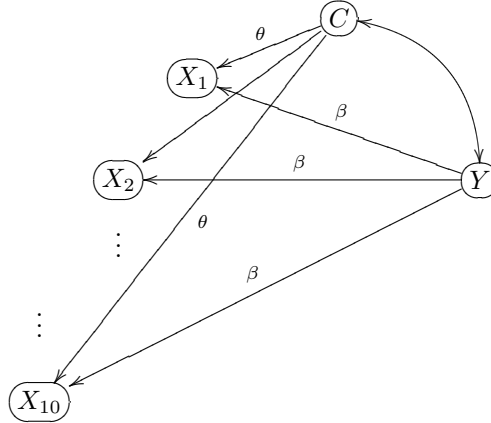
**Algorithm 2** Monte Carlo permutation null distribution to detect confounding

---

- 1: **Input:** Number of standard permutations,  $b_s$ ;  $\mathbf{X}$ ;  $\mathbf{y}$ ;  $\mathbf{c}$ ; training and test set indexes,  $i_{train}, i_{test}$
  - 2: Split  $\mathbf{X}$ ,  $\mathbf{y}$  and  $\mathbf{c}$  into training and test sets
  - 3: Set the number of restricted permutations to the test set size,  $b_r \leftarrow \text{Length}(i_{test})$
  - 4: **for**  $i = 1, 2, \dots, b_s$  **do**
  - 5:      $\mathbf{c}_{train}^{**} \leftarrow \text{StandardShuffle}(\mathbf{c}_{train}), \mathbf{c}_{test}^{**} \leftarrow \text{StandardShuffle}(\mathbf{c}_{test})$
  - 6:     **for**  $j = 1, 2, \dots, b_r$  **do**
  - 7:          $\mathbf{y}_{train}^* \leftarrow \text{RestrictedShuffle}(\mathbf{y}_{train}, \mathbf{c}_{train}^{**}), \mathbf{y}_{test}^* \leftarrow \text{RestrictedShuffle}(\mathbf{y}_{test}, \mathbf{c}_{test}^{**})$
  - 8:         Train a machine learning algorithm on the  $\mathbf{X}_{train}$  and  $\mathbf{y}_{train}^*$  data
  - 9:         Evaluate the algorithm on the  $\mathbf{X}_{test}$  and  $\mathbf{y}_{test}^*$  data
  - 10:         Record the value of the performance metric,  $m_j^*$ , on the shuffled data
  - 11:     **end for**
  - 12:     Compute and store  $\bar{m}_i^* = b_r^{-1} \sum_{j=1}^{b_r} m_j^*$
  - 13: **end for**
  - 14: **Output:**  $\bar{m}_1^*, \bar{m}_2^*, \dots, \bar{m}_{b_s}^*$
- 

### 8. Synthetic data generation for binary classification illustrations

In the simulation study and synthetic data illustrations for the binary classification problem (Figure 3 in the main text, and Figures S1 and S5) we simulate data according to the model,



where  $C$  represents a binary confounder,  $Y$  represents the disease status, and  $X_1, \dots, X_{10}$  represent the features.

This model is motivated by the following example involving a Parkinson’s disease (PD) classification problem. Suppose that the data is unbalanced with respect to the gender ( $C$ ) of the participants, with most of the male participants having PD and most of the female participants being controls (so that gender is strongly associated with the disease status). Because males on average are taller than females, it is reasonable to expect that many of the

features extracted from the raw accelerometer data will likely be influenced by gender since taller participants tend to have larger step sizes, and different heel strikes and acceleration patterns than shorter participants (hence, we have  $C \rightarrow X_j$ ). Furthermore, because PD patients experience difficulty to walk, their acceleration patterns tend to be distinct from control participants (hence, we have  $Y \rightarrow X_j$ ). Therefore, it is reasonable to expect that the features will be influenced by disease status as well.

In order to generate an association between  $C$  and  $Y$  (i.e.,  $C \leftrightarrow Y$ ) we jointly sample these binary variables from a bivariate Bernoulli distribution[15], with probability density function given by,

$$p(Y, C) = p_{11}^{yc} p_{10}^{y(1-c)} p_{01}^{(1-y)c} p_{00}^{(1-y)(1-c)}, \quad (29)$$

where  $p_{ij} = P(Y = i, C = j)$ , and  $p_{11} + p_{10} + p_{01} + p_{00} = 1$ . Note that the covariance between  $Y$  and  $C$  is given by,

$$Cov(Y, C) = p_{11} p_{00} - p_{01} p_{10}, \quad (30)$$

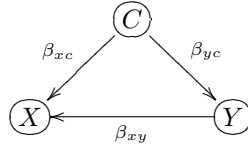
and we can tune the strength of the association between  $Y$  and  $C$  by changing these parameters. Once, we have sampled a  $\{y, c\}$  pair from this distribution, we sample the features from a multivariate normal distribution,

$$N_{10}((y\beta + c\theta)\mathbf{1}, \mathbf{\Sigma}), \quad (31)$$

where  $\mathbf{1}$  represents the vector of ones, and  $\mathbf{\Sigma}$  represents a correlation matrix with  $ij$ th element given by  $\rho^{|i-j|}$ .

## 9. Synthetic data generation for correlation metric illustrations

For the correlation illustrations, presented on Figure 2 in the main text, we simulated data from the model,



where  $C$  is a binary confounder sampled from a Bernoulli distribution with probability of success  $p$ ;  $Y$  is sampled from a  $N(\beta_{yc} c, 1)$ ; and  $X$  is sampled from a  $N(\beta_{xc} c + \beta_{xy} y, 1)$ . For each of the 1,000 simulations we used a distinct set of simulation parameters ( $p, \beta_{xc}, \beta_{yc}$ , and  $\beta_{xy}$ ), randomly draw from uniform distributions with ranges,

$$p \sim U(0.3, 0.7), \quad \beta_{xc} \sim U(-3, 3), \quad \beta_{yc} \sim U(-3, 3), \quad \beta_{xy} \sim U(-3, 3),$$

and sample size 1,000.

## 10. Simulation experiments

We performed four simulation experiments based on data generated under:  $H_1^*$  and  $H_1^c$ ;  $H_1^*$  and  $H_0^c$ ;  $H_0^*$  and  $H_1^c$ ; and  $H_0^*$  and  $H_0^c$ . In each experiment we generated 1,000 data sets. Each data set was generated (as described in Section 8) using a unique combination

of simulation parameter values. The following table presents the ranges of the simulation parameter values employed in each experiment.

parameter	experiment 1 $H_1^*, H_1^c$	experiment 2 $H_1^*, H_0^c$	experiment 3 $H_0^*, H_1^c$	experiment 4 $H_0^*, H_0^c$
$n$	$\{200, \dots, 600\}$	$\{200, \dots, 600\}$	$\{200, \dots, 600\}$	$\{200, \dots, 600\}$
$p_{11}$	$[0.40, 0.45]$	$[0.40, 0.45]$	$[0.40, 0.45]$	$[0.40, 0.45]$
$p_{00}$	$[0.40, 0.45]$	$[0.40, 0.45]$	$[0.40, 0.45]$	$[0.40, 0.45]$
$p_{10}$	$[0.050, 0.075]$	$p_{11}$	$[0.050, 0.075]$	$p_{11}$
$p_{01}$	$1 - p_{11} - p_{00} - p_{10}$	$p_{00}$	$1 - p_{11} - p_{00} - p_{10}$	$p_{00}$
$\beta$	$[0.1, 1.0]$	$[0.1, 1.0]$	0	0
$\theta$	$[0.1, 1.0]$	0	$[0.1, 1.0]$	0
$\rho$	$[0.2, 0.8]$	$[0.2, 0.8]$	$[0.2, 0.8]$	$[0.2, 0.8]$

(Note that in experiments 2 and 4, the probabilities  $p_{11}, p_{10}, p_{01}, p_{00}$  are re-normalized to sum 1.)

In order to select parameter values spread as uniformly as possible over the entire parameter range we employed a Latin hypercube design[16], optimized according to the maximin distance criterion[17], in the determination of the parameter values used in the generation of each synthetic data set.

### 11. Supplementary figures

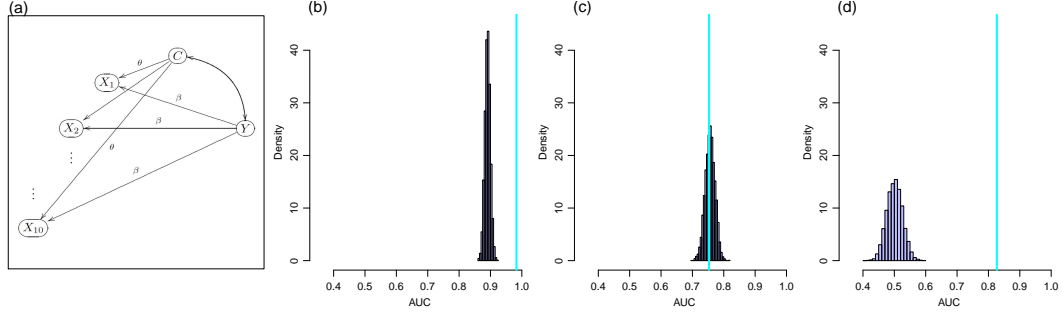


FIG S1. This figure illustrates the generation of the restricted Monte Carlo permutation null for the AUC metric using synthetic data. Panel a shows the causal graph representing the model used to simulate the data. (Details about this model are provided in Section 8.) Panels b-d show the restricted Monte Carlo permutation null distributions (blue histograms) for data generated with distinct strengths of confounding. The cyan lines represent the observed AUC values. In panel b, we simulated a very strong association between  $C$  and  $Y$  ( $\hat{c}o\hat{r}(C, Y) = 0.8$ ), and causal influences of  $C$  on  $\mathbf{X}$  ( $\theta = 1$ ), and of  $Y$  on  $\mathbf{X}$  ( $\beta = 1$ ). The restricted null is located close to 0.9, far away from the baseline random guess value (0.5 for the AUC metric), but still below the observed AUC value (cyan line around 0.98). This shows that while a lot of the predictive performance of the classifier is explained by the confounder, the direct association between  $Y$  and  $\mathbf{X}$  also contributes to it. Hence, in this example, the classifier was still able to learn the disease signal, in spite of the strong confounding influence. In this example, the permutation  $p$ -value for testing  $H_0^*$  vs  $H_1^*$  is smaller than  $9.9 \times 10^{-5}$  (we used 10,000 permutations to generate the null). In panel c, we simulated moderate/strong association between  $C$  and  $Y$  ( $\hat{c}o\hat{r}(C, Y) = 0.6$ ) and a causal influence of  $C$  on  $\mathbf{X}$  ( $\theta = 1$ ), but not of  $Y$  on  $\mathbf{X}$  ( $\beta = 0$ ). In this case while the restricted null is, again, located far way from 0.5, the observed AUC score (cyan line around 0.75) is located inside the range of the permutation null showing that the classifier is detecting the confounding signal, but not the response signal (as expected since we set  $\beta = 0$  in this example). In this example, the permutation  $p$ -value is 0.59. Finally, in panel d we simulated data with causal influences of  $C$  on  $\mathbf{X}$  ( $\theta = 1$ ) and  $Y$  on  $\mathbf{X}$  ( $\beta = 1$ ), but no association between  $C$  and  $Y$  (that is, we generated unconfounded data). As, expected, the restricted permutation distribution is centered around 0.5, while the observed AUC is above 0.8. These examples illustrate that the restricted permutation null is centered away from the baseline random guess value whenever confounding is present (and that this shift can be used to informally infer the presence of confounding).

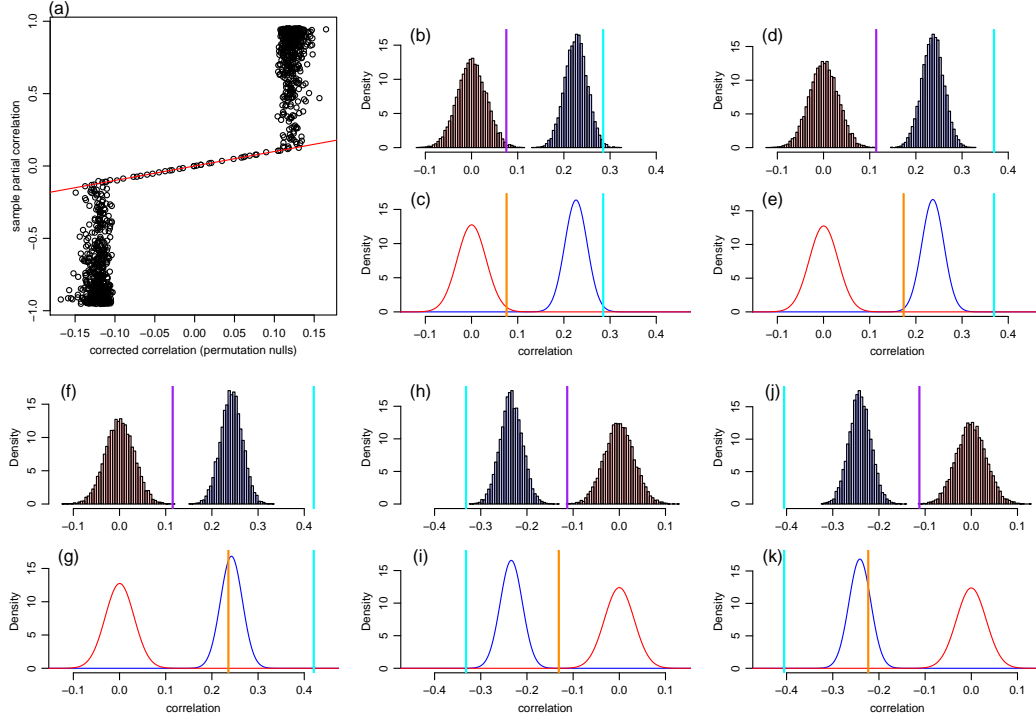


FIG S2. Comparison of partial correlation and corrected correlation values across 1,000 simulated data sets (generated as described in Section 9). Panel a compares the corrected correlation value (x-axis), computed with the formula  $\hat{m}_c = \hat{F}_{\hat{\pi}^{**}}^{-1}(\hat{F}_{\hat{\pi}^{**}}(m_o))$ , against the partial correlation estimated using the standard partial correlation formula (y-axis). The red line represents the identity line, where the corrected correlation score exactly matches the partial correlation score. Note that for some of the simulated data sets the two formulas provide very close scores, while, for most of the simulations, the corrected correlation tends to be truncated around  $-0.12$  and  $0.12$ . Panels b-k explain why. In all panels, the blue and red histograms represent, respectively, the restricted and standard permutation null distribution, while the blue and red bell shaped curves represent the respective normal approximations. The cyan line represents the observed correlation score. The purple line represents the corrected correlation, computed using  $\hat{m}_c = \hat{F}_{\hat{\pi}^{**}}^{-1}(\hat{F}_{\hat{\pi}^{**}}(m_o))$  (and from now on denoted as the “purple” correction), while the orange line represents correlations corrected according to the formula  $\hat{m}_c = (m_o - a_{\hat{\pi}^{**}})s_{\hat{\pi}^{**}}/s_{\hat{\pi}^{**}} + a_{\hat{\pi}^{**}}$  (denoted “orange” correction). Points falling at the red line in panel a represent simulations where the observed correlation score falls inside the range of the restricted permutation null, as illustrated in panels b and c. (Note how the purple line in panel b matches the orange line in panel c). Panel d shows the case where the observed correlation falls above the range of the restricted permutation null. In this case, the corrected value (purple line) corresponds to the upper boundary of the red histogram since  $\hat{F}_{\hat{\pi}^{**}}(m_o) = 1$  for any observed correlation value above the range of the blue histogram and  $\hat{F}_{\hat{\pi}^{**}}^{-1}(1)$  corresponds to the upper boundary of the red histogram. Note, however, that the corrected value based on the asymptotic approximation (orange line in panel e) is higher than the purple line. Panel f shows an example where the observed correlation is even larger, but the “purple” corrected value is still similar to the previous example (compare the purple lines in panels d and f). The “orange” corrected value, on the other hand, is larger (compare the orange lines in panels e and g). The examples in panels b-g illustrate why the corrected values computed with  $\hat{m}_c = \hat{F}_{\hat{\pi}^{**}}^{-1}(\hat{F}_{\hat{\pi}^{**}}(m_o))$  get truncated around  $0.12$  in panel a. Similarly, panels h-k illustrate that, when the observed correlation is negative, the “purple” corrected values correspond to the minimum of the standard permutation null distributions (since  $\hat{F}_{\hat{\pi}^{**}}(m_o) = 0$  and  $\hat{F}_{\hat{\pi}^{**}}^{-1}(0)$  corresponds to the lower boundary of the standard permutation null). Hence, we also observe a truncation of the “purple” corrected correlations around  $-0.12$  in panel a. Finally, note that the asymptotic approximation fixed this issue, so that the “orange” corrected correlations closely approximate the partial correlations (as illustrated in Figure 3b in the main text).

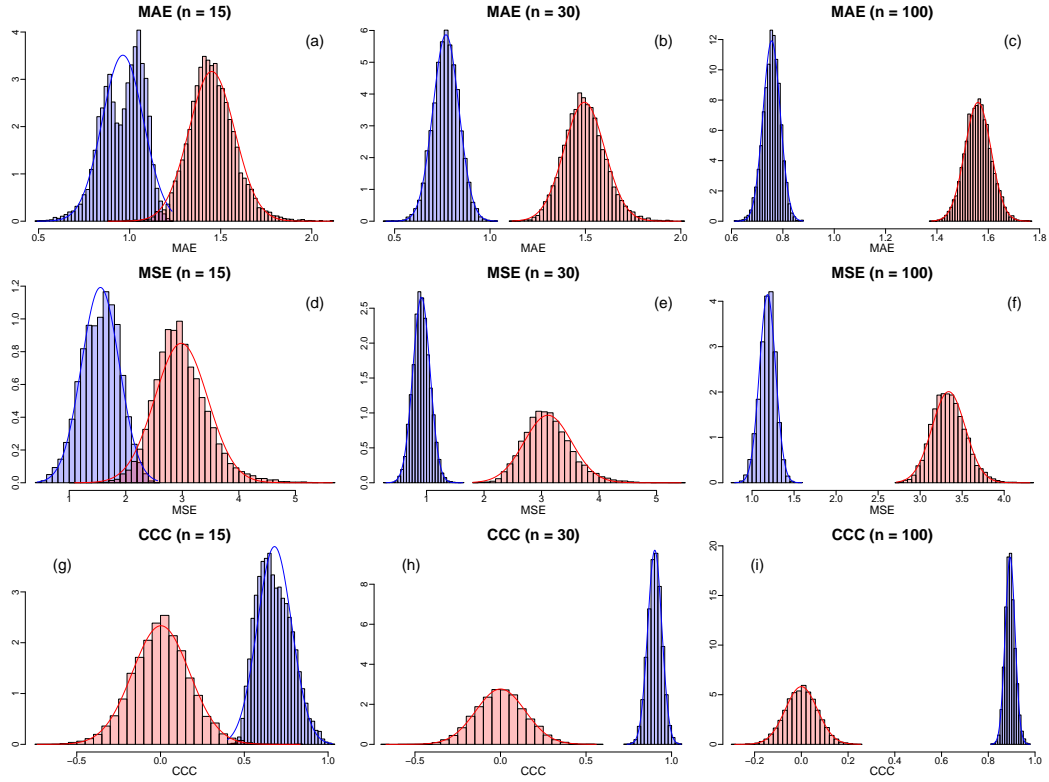


FIG S3. Asymptotic normality of common performance metrics for regression problems. Panel a, b and c show the restricted (blue histograms) and standard (red histograms) permutation null distributions for the mean absolute error (MAE) metric, generated using training and test sets of size 15, 30, and 100, respectively. Panels d, e, and f, show similar plots for the mean squared error (MSE) metric, while panels g, h, and i, show the same plots for the concordance correlation coefficient (CCC) metric. The data was simulated as described before (Section 9) except that we adopted exponential instead of gaussian errors for the generation of the response. For all metrics we observe a poor approximation for test sets with 15 samples, but reasonable approximations for test sets with 30 or 100 samples.

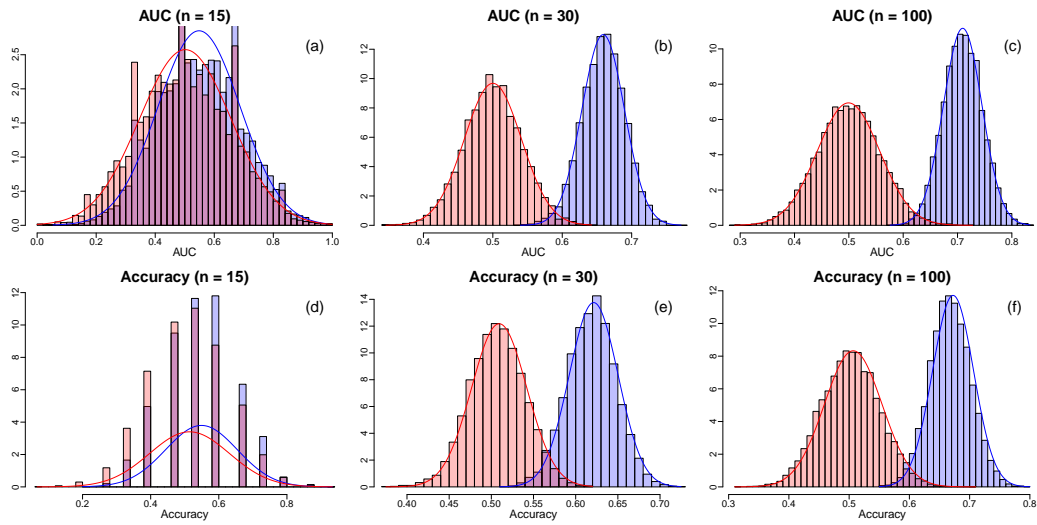


FIG S4. Asymptotic normality of common performance metrics for classification problems. Panel a, b and c show the restricted (blue histograms) and standard (red histograms) permutation null distributions for the AUC metric, generated with training and test sets of size 15, 30, and 100, respectively. Panels d, e, and f, show similar plots for the accuracy metric. The data was simulated as described in Section 8. For all metrics we observe a poor approximation for test sets with 15 samples (note the discreteness of the permutation distributions), but reasonable approximations for test sets with 30 or 100 samples.

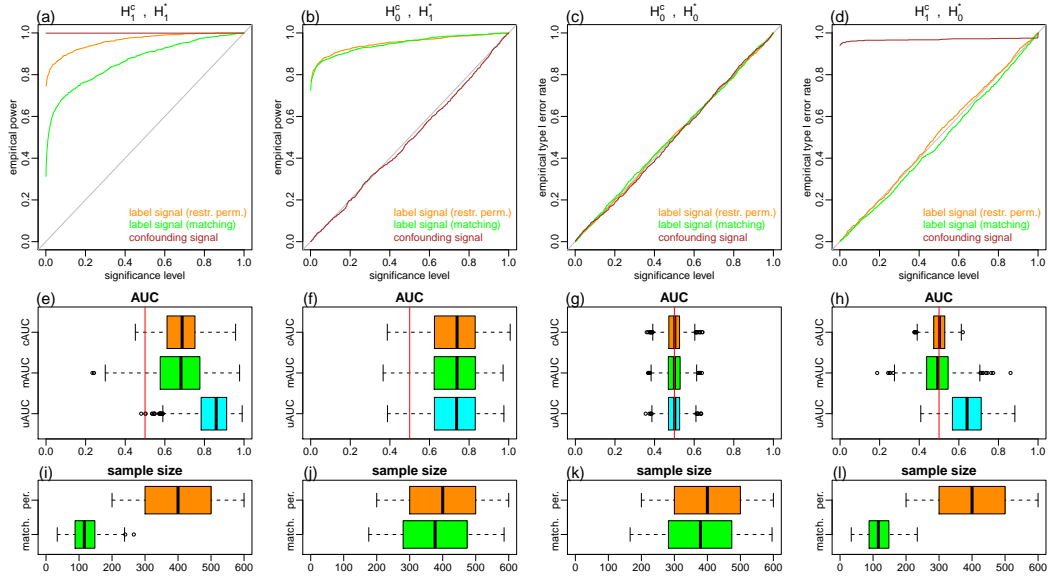


FIG S5. Comparison of matching vs the proposed confounder correction approach using synthetic data sets. In this figure we included the matching approach results obtained using the same synthetic data sets employed in the four simulation experiments presented in the main text. Panels a and b show the empirical power for the permutation (orange curve) and matching (green curve) approaches in the presence (panel a) and absence (panel b) of confounding. Note that in the presence of confounding the permutation approach is better powered to detect response learning (due to larger sample sizes as shown in panel i). In the absence of confounding (panel b), the matching approach discards very few samples (see panel j) and end up achieving similar empirical power to the permutation approach. Panels c and d report the empirical type I error rates achieved in the presence (panel d) and absence (panel c) of confounding. In both cases the type I error rates are well controlled at the nominal significance levels. Panels e-h show the distributions of the permutation corrected (orange), matching (green), and observed (cyan) AUCs for each of the respective simulation experiments. In the presence of confounding (panels e and h), the corrected and matching AUCs were lower than the observed AUCs. The similar medians of the orange and green boxplots suggest that, on average, these two approaches generate similar AUCs under the particular conditions investigated in these simulations (i.e., sample sizes, strengths of the confounding and response signals, etc). The larger spread of the green boxplots indicates that the AUC estimates obtained with matching tend to be noisier due to the smaller sample sizes. In the absence of confounding (panels f and g), all approaches generate similar AUC values. Note, as well, that under  $H_0^*$  the corrected AUCs were distributed around 0.5 (panels g and h), while in panel h the observed AUCs were still above of 0.5 due to confounding. Panels i-l report the distributions of the combined sample sizes of training and test sets across the four simulation experiments.